

透过率起伏相关频谱法测量两相流场中颗粒速度、粒径分布和体积分数

龚鹏, 沈建琪*

上海理工大学理学院, 上海 200093

摘要 两相流中颗粒的运动速度、粒径分布和体积分数是非常重要的参数。本文介绍了一种基于透过率起伏相关频谱测试技术的光学测量装置,并采用该装置实现了颗粒运动速度、粒径分布和体积分数的同时测量。该测试装置具有结构简单、易实现和便于安装维护等特点,有望应用于两相流的在线实时测量。实验结果与标称直径、其他测量方法所得结果相符并具有较好的重复性,证明了测试装置的可行性。

关键词 测量; 两相流; 透过率起伏相关频谱; 颗粒粒径分布

中图分类号 O436

文献标志码 A

DOI: 10.3788/CJL202249.2304005

1 引言

颗粒两相流广泛存在于能源、工业、环境等领域。两相流场中颗粒的尺寸分布、体积分数和速度等参数的测量至关重要。在燃煤发电行业中,一般需要将燃煤磨至一定的粒径范围,太大的煤粉颗粒会导致燃烧器之间的颗粒流动分布不均匀并会导致相关的燃烧问题,而太小的颗粒会在通气过程中被气流带走造成原料浪费。因此,煤粉颗粒的粒径应分布在可接受的范围内,以确保燃烧过程,有效提高燃煤的燃烧效率同时降低污染物的排放浓度^[1-5]。在采矿尾矿处理及悬沙输运过程中,及时掌握颗粒的粒径、速度或悬浮物浓度的变化有助于输运的完成并减少事故的发生^[6]。颗粒粒径参数的有效表征在石料粉碎^[7]、饲料加工^[8]、河床泥沙流动^[9]等场合也起着至关重要的作用。目前,线下检测技术已不能满足工业发展的要求,有必要发展实时、在线检测两相流场中颗粒相关参数的技术。

随着测量技术的发展,许多新的基于不同测量原理和方法的测量技术已被提出并用于在线测量,如超声法、图像法、电感应法、光纤传感法、相位多普勒粒子分析技术、数字全息技术等。Yu 等^[10]利用多频超声频谱衰减法通过测量液固分散系中颗粒的粒度和浓度来模拟管道中颗粒的输运情况。Chen 等^[11]提出了一种图像处理方法,用于测量稀释两相流中颗粒的粒径、速度和体积分数。Xiao 等^[12]采用光学光纤对锥阀内固体颗粒的流动特性进行了实验研究,并给出了床层物料颗粒的粒径分布。den Moortel 等^[13]采用相位多普勒粒子分析仪对循环流化床内的气固颗粒流动进行

了实验研究。Prasad 等^[14]利用数字在线全息技术对粉尘中的粒子密度进行了测量。

各种在线测量方法或仪器均与应用场景密切相关并存在一定的局限性。譬如:超声衰减法可应用于极高体积分数的两相流测量,但其要求掌握较多的物性参数,并且在线测量往往受到外部各种噪声的影响^[15];图像法和数字全息技术适用于体积分数较低的颗粒两相流,且数据分析速度较慢;相位多普勒粒子分析仪价格昂贵,不适于广泛推广。

透过率起伏自相关频谱法(TFS-AC)是一种利用透过率起伏信号的自相关特征获取颗粒粒度分布和体积分数的光学测量技术。Shen 等^[16-18]提出了一种用一束会聚高斯光束在束腰区获得较窄光束从而达到对较小颗粒进行测量目的的方法,但该方法需采用额外的测试手段得到速度信息。本文介绍了一种简单的分束装置,用于实现透过率起伏相关频谱测试。该装置采用平行光照射颗粒,采集两路透过率起伏信号,然后通过互相关计算获得颗粒的速度信息,采用单路透过率起伏信号获得自相关频谱再进行反演计算得到颗粒的粒径分布和体积分数。该实验装置简单、价格便宜、易于安装、可重复性强,有望应用于颗粒两相流在线测量。

2 测量原理

透过率起伏相关频谱法的测试原理^[19-20]如图 1 所示。两束粗细相同的窄光束相互平行,颗粒流动方向在光束所在平面内且垂直于光束传播方向。两束窄光束的直径均为 D_B ,光束中心间距为 L ,采用两个 PIN

管探测光强信号并进行放大处理。当光束中不存在颗粒时,探测到的光强信号为入射光强度 $I_{1,0}$ 和 $I_{2,0}$;当颗粒随机流经测量区时,得到随时间变化的信号 $I_1(t)$ 和 $I_2(t)$ 。因此,两路透过率信号分别为 $T_1(t)=I_1(t)/I_{1,0}$ 和 $T_2(t)=I_2(t)/I_{2,0}$ 。

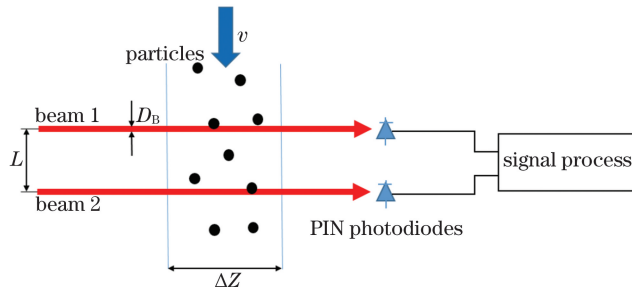


图 1 透过率起伏相关频谱法测量原理图

Fig. 1 Measurement principle diagram of transmission fluctuation correlation spectrometry

2.1 速度测量

对两路透过率起伏信号作互相关计算可得到颗粒的流速。互相关信号的计算公式为

$$E_{L,\tau} = e\{T_1(t)T_2(t+\tau)\} = \lim_{t_s \rightarrow \infty} \frac{1}{t_s} \int_{0}^{t_s} T_1(t)T_2(t+\tau) dt, \quad (1)$$

式中: $e\{\cdot\}$ 表示期望值; τ 为相关时间; t_s 为信号采样时间。改变相关时间 τ ,并将互相关信号 $E_{L,\tau}$ 达到最大时对应的 τ 值记作 τ_{peak} ,将 τ_{peak} 与两光束的距离 L 结合起来即可得到颗粒的速度,即

$$v = \frac{L}{\tau_{peak}}. \quad (2)$$

2.2 颗粒粒径及体积分数的测量

任取其中一路透过率起伏信号 $T_k(t)$ (其中 $k=1,2$)进行自相关计算,自相关信号的计算公式为

$$E = e\{T_k(t)T_k(t+\tau)\} = \lim_{t_s \rightarrow \infty} \frac{1}{t_s} \int_{0}^{t_s} T_k(t)T_k(t+\tau) dt. \quad (3)$$

当相关时间 $\tau=0$ 时, $T_k(t)=T_k(t+\tau)$,因此自相关信号实际上是透过率起伏信号 $T_k(t)$ 平方的期望值。随着相关时间 τ 增大, $T_k(t)$ 与 $T_k(t+\tau)$ 之间的相关性逐渐降低;当相关时间 $\tau>(x+D_B)/v$ (其中 x 是颗粒粒径)时, $T_k(t)$ 与 $T_k(t+\tau)$ 之间不再相关。因此,改变自相关时间 τ 可以得到透过率乘积期望值与相关时间 τ 的关系,即颗粒透过率起伏自相关频谱。

对于多分散颗粒体系^[18],透过率起伏自相关频谱可以表示为

$$-\ln E(\tau_i) = \sum_{j=1}^n \frac{1.5\Delta Z}{\bar{x}_j} [2 - \chi(\Delta_{i,j}, \Lambda_j)] \cdot C_v(\bar{x}_j) \Delta x_j, \quad (4)$$

式中: n 为颗粒粒径的分档数; \bar{x}_j 为第 j 分档区间内颗粒的平均粒径; Δx_j 为颗粒粒径分档宽度; $C_v(\bar{x}_j)$ 为颗粒的体积分数; ΔZ 为测量区光程; τ_i ($i=1,2,\dots,m$) 为自相关时间; $\chi(\Delta_{i,j}, \Lambda_j)$ 为透过率起伏自相关频谱特征函数; $\Delta_{i,j}=v \cdot \tau_i / \bar{x}_j$ 是与自相关时间有关的无因次参数; Λ_j 是光束直径与颗粒粒径的比值, $\Lambda_j=D_B/\bar{x}_j$ 。

对于图 1 所示的准直光束,假设光束横截面内的光强分布均匀,颗粒为球形,则透过率起伏自相关频谱特征函数可表示为

$$\chi(\Delta, \Lambda) = \int_0^\infty J_0(2u\Delta) \left[\frac{2J_1(u\Lambda)}{u\Lambda} \right]^2 \frac{2J_1(u\Delta)}{u} du, \quad (5)$$

式中: J_0 表示零阶贝塞尔函数; u 表示为积分变量; J_1 表示一阶贝塞尔函数。

式(4)可以写成

$$\sum_{j=1}^n M_{i,j} X_j = Y_i, \quad (6)$$

式中: Y_i 是测量得到的透过率起伏自相关频谱, $Y_i=-\ln E(\tau_i)$; X_j 代表颗粒粒径分布, $X_j=C_v(\bar{x}_j) \Delta x_j / \bar{x}_j$; $M_{i,j}=1.5\Delta Z [2-\chi(\Delta_{i,j}, \Lambda_j)]$ 。它们均可通过式(5)计算得到。

利用反演算法^[21-25]对式(6)进行求解就可得到颗粒的粒径分布。此外,还可以计算得到多分散颗粒系的体积分数 C_v ,计算公式为

$$C_v = \sum_{j=1}^n C_v(\bar{x}_j) \cdot \Delta x_j. \quad (7)$$

3 实验

3.1 实验装置

实验装置如图 2 所示。样品池与 BT-800 自动循环分散器通过塑料软管连接构成循环分散系统,循环分散器中装有一定体积配比的固体颗粒水溶液。当循环分散系统达到稳定循环后,水溶液中的颗粒随水流一起流动。样品池测量区光程 $\Delta Z=2$ mm,He-Ne 激光器($\lambda=0.6328$ μm)发出的激光束在扩束准直后垂直照射到样品池上,透过颗粒系后的光束照射到挡光板上,挡光板上开有两个小孔,小孔直径为 850 μm,小孔中心间距为 1.4 mm。在挡光板后放置双元光电二极管 S4204,其截止频率为 30 MHz,每个光电二极管的有效受光截面尺寸为 1 mm×1 mm,两个光电二极管受光面之间的距离为 0.02 mm。实验中采用的是 PCI-50612(12 bit)数据采集卡,其支持的每通道最高采样率为 50 MSa/s。透射光信号经过小孔后被双元光电二极管接收,经信号放大系统放大后由数据采集卡采集,然后传输到计算机中进行后续处理。

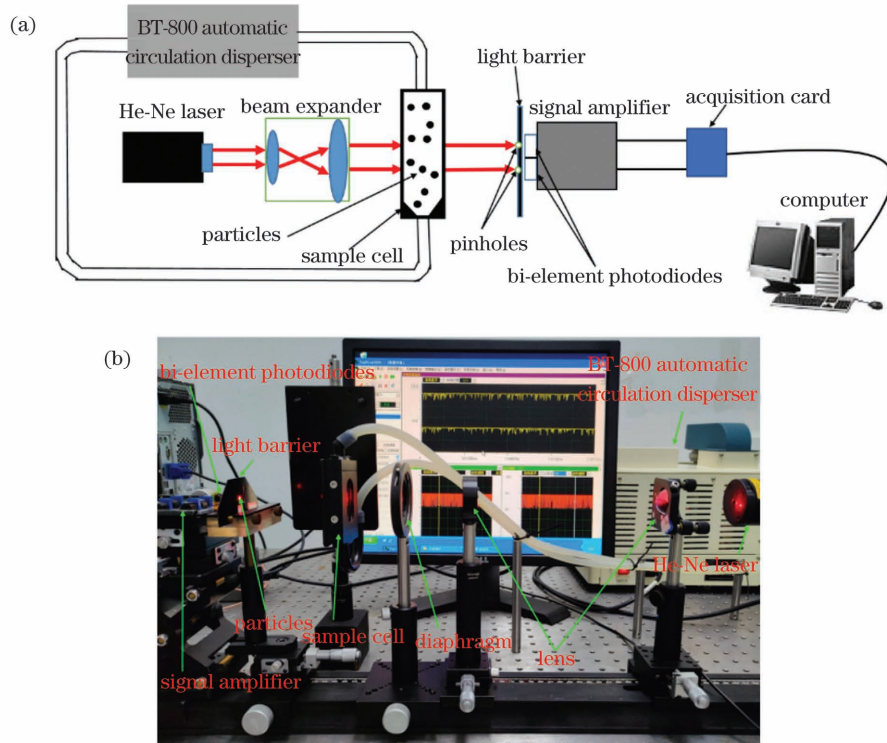


图 2 实验装置。(a)实验装置示意图;(b)实验装置实物图

Fig. 2 Experimental setup. (a) Schematic of experimental setup; (b) photo of experimental setup

3.2 实验结果

对不同粒径的球形玻璃珠、非球形石英砂和白刚玉颗粒进行测量。其中:玻璃珠的标称直径分别为 200、400、500、700 μm ,密度为 $2.45 \times 10^3 \text{ kg/m}^3$;石英砂颗粒的标称直径为 200 μm ,密度为 $2.65 \times 10^3 \text{ kg/m}^3$;白刚玉颗粒的标称直径为 600 μm ,密度为 $3.95 \times 10^3 \text{ kg/m}^3$ 。将待测颗粒样品称重后按一定比例进行混合,然后倒入循环分散器中。根据颗粒密度可折算出颗粒在两相流中的体积分数。为防止循环流动过程中颗粒沉降,将 BT-800 自动循环分散器的转速设置为 800 r/min,利用激光测速仪(TM680)测得该转速下玻璃珠颗粒在测量区中的流速为 1.15 m/s。

在所有颗粒样品测试过程中,数据采集卡的采样频率设置为 125 kHz,采集长度为 512 kB,则采集时长为 4.096 s。两路透过率信号分别写成 $T_{1,i}$ 和 $T_{2,i}$,其中 $i=1, 2, \dots, N, N=2^{19}$ 。单次测量采集 524288 个数据点,在计算透过率起伏相关谱和透过率期望值时误差小于 0.14%。因此,式(1)和式(3)所示的互相关和自相关计算可以写成式(8)和式(9)的形式。

$$E_{L,\tau} = \frac{1}{N} \sum_{i=1}^N T_{1,i} T_{2,i+\tau}, \quad (8)$$

$$E_\tau = \frac{1}{N} \sum_{i=1}^N T_{k,i} T_{k,i+\tau}, \quad (9)$$

式中: $k=1$ 或 $k=2$,对应任意信号 1 或 2;相关时间为 $\tau=j \cdot \Delta_s, \Delta_s=8 \mu\text{s}$ 取决于采样频率。在个人计算机(i5-4900,CPU@3.30 GHz+RAM@8.00 GB)上对采

集的透过率信号进行相关处理和反演计算^[21-25]。两路透过率信号的互相关处理和单路信号的自相关处理均采用快速傅里叶变换(FFT),互相关处理后得到颗粒流经测量区的速度信息,自相关处理后得到透过率起伏自相关谱。本文采用改进的 Chahine 循环算法^[21-22]对透过率起伏自相关谱进行反演计算,得到颗粒的粒径分布和体积分数。单组测量数据的整个数据处理过程可在 3~5 s 内完成。

图 3(a)给出了表 1 中标称直径为 700 μm 的玻璃珠的第 3 组测量数据的透过率起伏互相关频谱曲线,其中横坐标 j 代表延迟量,单个延迟量对应的相关时间为 8 μs (取决于设定的采样频率),纵坐标 $E_{L,j}$ 表示互相关值。在图 3(a)中,互相关谱 $E_{L,j}$ 的峰值出现在 $j=154$ 处,对应的相关时间为 $\tau_{\text{peak}} = j \cdot \Delta_s = 1.232 \text{ ms}$ 。根据两路光束中心距离 L 可得颗粒流速约为 1.136 m/s。图 3(b)是单路信号透过率起伏自相关频谱,横坐标为相关时间,纵坐标为透过率自相关函数的负对数。随着相关时间变化,自相关信号出现特征性变化,其中含有颗粒的粒径信息;自相关信号的高度包含了颗粒体积分数的相关信息。

表 1 给出了球形玻璃珠、非球形石英砂和白刚玉颗粒在循环分散器作用下的速度测试结果。可以看出,由透过率信号互相关处理得到的玻璃珠颗粒和石英砂颗粒的速度与激光测速仪测试得到的结果吻合,但白刚玉颗粒的运动速度明显偏小。这是因为白刚玉颗粒的密度远大于水的密度,不易随流体循环运动。

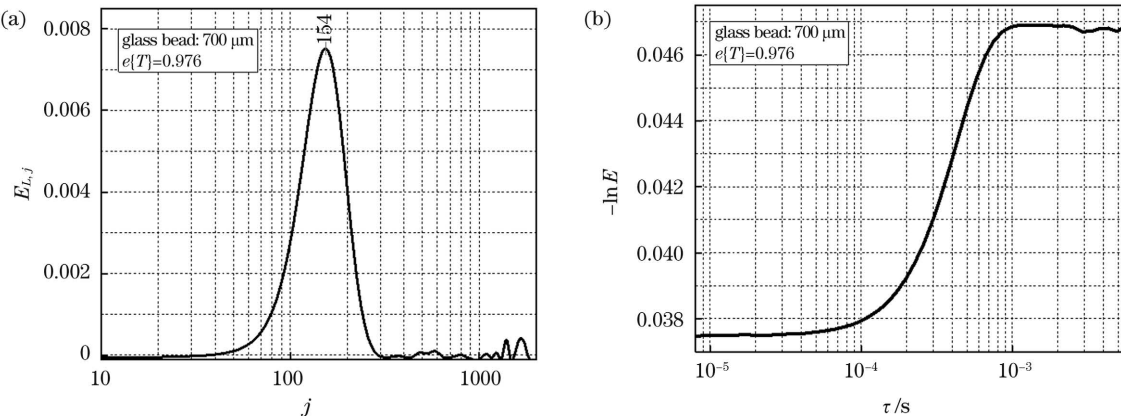


图 3 标称直径为 $700 \mu\text{m}$ 的玻璃珠的相关频谱。(a)透过率起伏互相关频谱;(b)透过率起伏自相关频谱

Fig. 3 Correlation spectra of glass beads with nominal size of $700 \mu\text{m}$. (a) Cross-correlation spectrum of transmission fluctuation; (b) auto-correlation spectrum of transmission fluctuation

表 1 循环分散器中颗粒运动速度的测量结果

Table 1 Measurement results of particle velocity in circulating disperser

No.	Particle velocity/($\text{m} \cdot \text{s}^{-1}$)					
	Glass bead with 200 μm nominal diameter	Glass bead with 400 μm nominal diameter	Glass bead with 500 μm nominal diameter	Glass bead with 700 μm nominal diameter	Silica sand with 200 μm nominal diameter	White corundum with 600 μm nominal diameter
1	1.207	1.167	1.182	1.159	1.136	1.054
2	1.151	1.159	1.159	1.151	1.159	1.087
3	1.159	1.144	1.167	1.136	1.174	1.042
4	1.136	1.144	1.136	1.122	1.151	1.042
5	1.151	1.136	1.136	1.129	1.122	1.042
6	1.159	1.129	1.136	1.212	1.136	1.029
Average value	1.161	1.146	1.153	1.137	1.147	1.049

图 4 所示为改进的 Chahine 循环反演算法流程图。反演步骤如下:1) 输入理论计算得到的模式矩阵 $\mathbf{M}_{i,j}$;2) 预设颗粒粒径分布 $X_j^{(0)} = 1$, 其中 $j = 1, 2, \dots, n$;3) 根据颗粒的粒径分布, 计算透过率自相关频谱 $Y_{\text{calc},i}$, 并将其与透过率自相关频谱测试值 $Y_{\text{meas},i}$

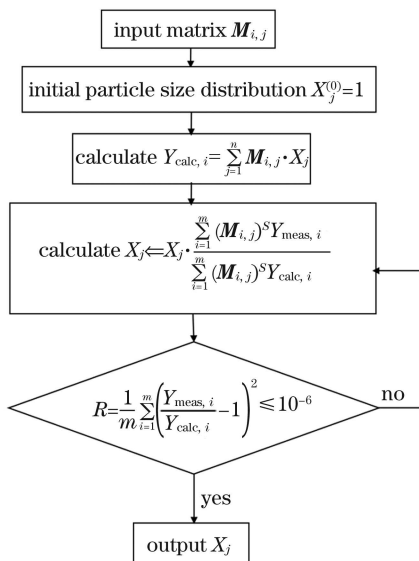


图 4 改进的 Chahine 反演计算流程图

Fig. 4 Chart of modified Chahine iterative algorithm

进行比较, 确定下一步循环中 X_j 的修正系数(为了加速迭代收敛速度, 引进加速参数 S);4) 当 $Y_{\text{calc},i}$ 与 $Y_{\text{meas},i}$ 之间的残差满足设定的阈值时, 结束循环, 否则, 返回上一步继续循环。

图 5 给出了反演计算得到的不同体积分数下球形玻璃珠、非球形石英砂颗粒和白刚玉颗粒的累积分布曲线, 其中颗粒累积分布 $Q_3(\bar{x}_j)$ 根据反演计算得到的每个粒径区间的颗粒频度分布 $C_V(\bar{x}_j)$ 进行归一化计算后得到, 计算公式为

$$Q_3(\bar{x}_j) = \frac{\sum_{k=1}^j C_V(\bar{x}_k) \Delta x_k}{\sum_{k=1}^n C_V(\bar{x}_k) \Delta x_k} \quad (10)$$

每组样品的特征粒径(10%粒径 x_{10} 、中位粒径 x_{50} 和 90%粒径 x_{90})及其平均值列于表 2 中。由图 5 可以看出, 不同体积分数下测试得到的颗粒累积分布曲线大部分具有较好的重复性。200 μm 玻璃珠和石英砂颗粒在不同体积分数下的测试结果存在较为明显的偏差。由表 2 可知, 玻璃珠中位粒径 x_{50} 的平均值与标称粒径比较吻合, 石英砂颗粒和白刚玉颗粒中位粒径 x_{50} 的平均值测试结果稍大于其标称粒径。这是由于石英砂和白刚玉颗粒均属于非球形颗粒, 其粒径测试结

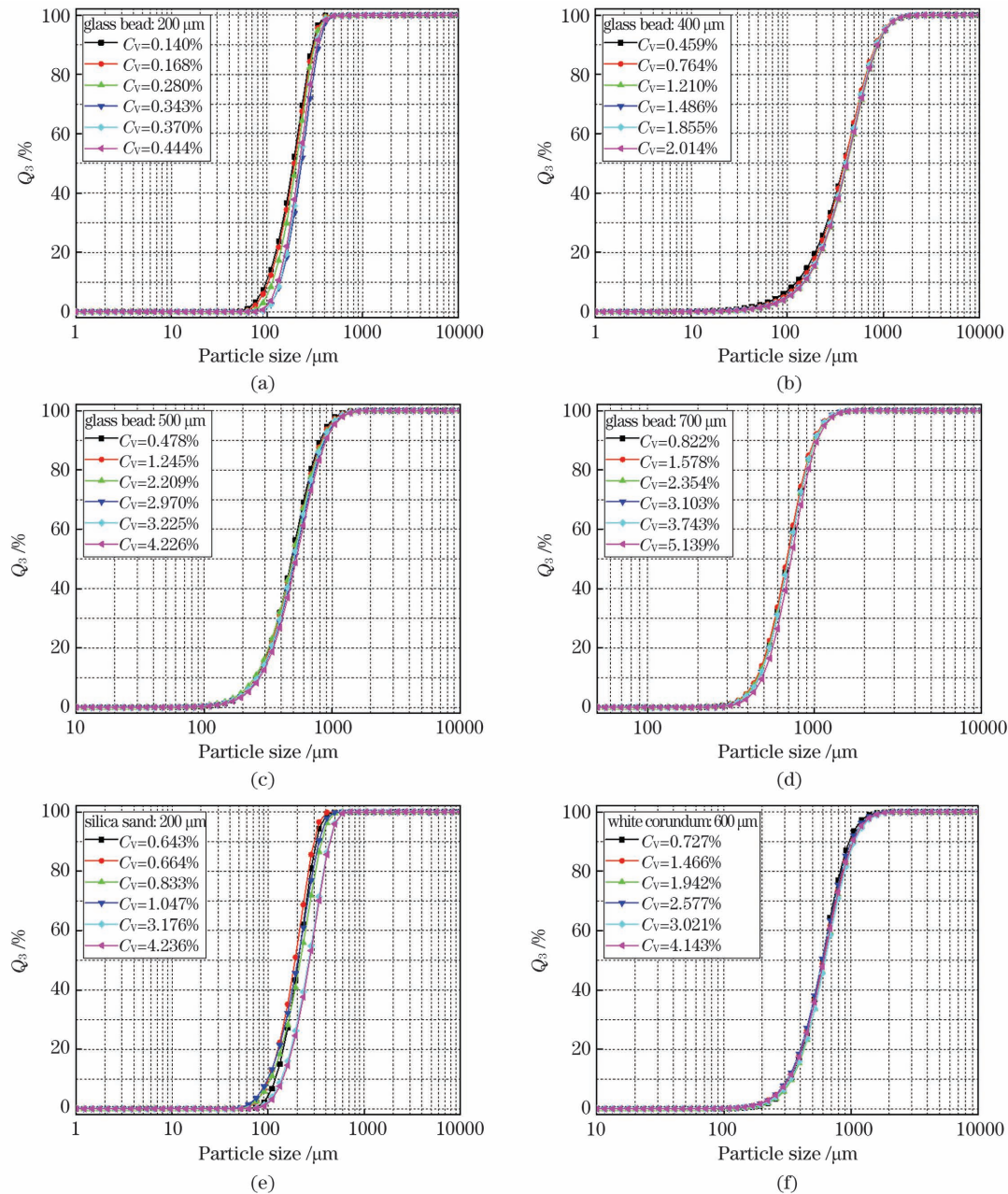


图5 不同体积分数下颗粒粒径的反演计算结果。(a)标称直径为200 μm的玻璃珠;(b)标称直径为400 μm的玻璃珠;(c)标称直径为500 μm的玻璃珠;(d)标称直径为700 μm的玻璃珠;(e)标称直径为200 μm的石英砂;(f)标称直径为600 μm的白刚玉

Fig. 5 Inversion results of particle size distributions for variant volume fraction. (a) Glass bead with 200 μm nominal diameter; (b) glass bead with 400 μm nominal diameter; (c) glass bead with 500 μm nominal diameter; (d) glass bead with 700 μm nominal diameter; (e) silica sand with 200 μm nominal diameter; (f) white corundum with 600 μm nominal diameter

表2 透过率起伏相关频谱法测量得到的特征粒径 x_{10} 、 x_{50} 和 x_{90}

Table 2 Characteristic particle size x_{10} , x_{50} and x_{90} measured with transmission fluctuation correlation spectrometry

Particle	$x_{10}/\mu\text{m}$						Average $x_{10}/\mu\text{m}$
Glass bead with 200 μm nominal diameter	98	103	114	138	136	130	120
Glass bead with 400 μm nominal diameter	125	136	152	146	148	150	143
Glass bead with 500 μm nominal diameter	257	258	248	263	261	272	260
Glass bead with 700 μm nominal diameter	457	451	459	467	467	488	465
Silica sand with 200 μm nominal diameter	119	102	106	99	137	142	117
White corundum with 600 μm nominal diameter	337	320	343	319	336	324	330

续表

Particle	$x_{50}/\mu\text{m}$						Average $x_{50}/\mu\text{m}$
Glass bead with 200 μm nominal diameter	188	192	201	228	220	217	208
Glass bead with 400 μm nominal diameter	390	393	421	412	408	416	407
Glass bead with 500 μm nominal diameter	482	491	489	510	503	525	500
Glass bead with 700 μm nominal diameter	692	684	697	699	698	724	699
Silica sand with 200 μm nominal diameter	207	190	216	204	265	270	225
White corundum with 600 μm nominal diameter	594	603	622	593	626	610	608
Particle	$x_{90}/\mu\text{m}$						Average $x_{90}/\mu\text{m}$
Glass bead with 200 μm nominal diameter	298	304	311	346	327	330	319
Glass bead with 400 μm nominal diameter	865	835	881	868	848	869	861
Glass bead with 500 μm nominal diameter	806	828	841	870	853	895	849
Glass bead with 700 μm nominal diameter	1006	1002	1013	1014	1005	1052	1015
Silica sand with 200 μm nominal diameter	314	299	359	337	333	338	330
White corundum with 600 μm nominal diameter	962	1030	1033	998	1061	1037	1020

果与颗粒经过测量区时颗粒在空间上的分布取向有关。

采用激光粒度仪 Bettersize2600 对所有颗粒样品的特征粒径进行测试,表 3 给出了特征粒径 x_{10} 、 x_{50} 和 x_{90} 的测试结果。从表 2 和表 3 可以看出,透过率起伏相关频谱法和激光粒度仪的测试结果均能得到较合理的 x_{50} 值,但激光粒度仪测试得到的 x_{50} 值与颗粒样品标称值偏离的程度相对较大。此外,比较两种测试方法所得的 x_{10} 和 x_{90} 值可以发现,激光粒度仪测试得到的颗粒粒径分布较窄,而透过率起伏相关频谱法得到的颗粒粒径分布偏宽。这是由于透过率起伏相关频谱法测试得到的颗粒粒径分布结果与颗粒通过测量区的速度有关。本次实验中,样品池的厚度为 2 mm,当颗粒流经测量区时,不同位置处颗粒的运动速度存在差异;同时,在测试过程中循环泵的脉动会导致流速不稳。这些因素均可导致颗粒粒径分布的测试结果偏宽。此外,激光粒度仪的测试原理与透过率起伏相关频谱法的原理也不同,这也是影响颗粒粒径分布宽度的因素。不过,从测试结果所呈现的规律看,两种方法所得结果与颗粒样品的标称值存在可比性。

颗粒的体积分数 C_V 可通过称重的方法进行确

表 3 Bettersize2600 测量得到的特征粒径 x_{10} 、 x_{50} 和 x_{90}

Table 3 Characteristic particle size x_{10} , x_{50} and x_{90} measured using Bettersize2600

Particle	$x_{10}/\mu\text{m}$	$x_{50}/\mu\text{m}$	$x_{90}/\mu\text{m}$
Glass bead with 200 μm nominal diameter	131	190	271
Glass bead with 400 μm nominal diameter	351	437	543
Glass bead with 500 μm nominal diameter	434	512	617
Glass bead with 700 μm nominal diameter	458	657	899
Silica sand with 200 μm nominal diameter	119	203	299
White corundum with 600 μm nominal diameter	208	584	875

$$C_{V_{\text{mass}}} = \frac{m}{\rho V}, \quad (11)$$

式中: m 是颗粒的质量,单位为 kg; ρ 是颗粒的密度,单位为 kg/m^3 ; V 是颗粒和分散液的总体积,单位为 m^3 。图 6 给出了透过率起伏自相关频谱法测试得到的颗粒体积分数 $C_{V_{\text{TFS-AC}}}$ 和称重法得到的颗粒体积分数 $C_{V_{\text{mass}}}$ 的比较。从测量结果可以看出,透过率起伏

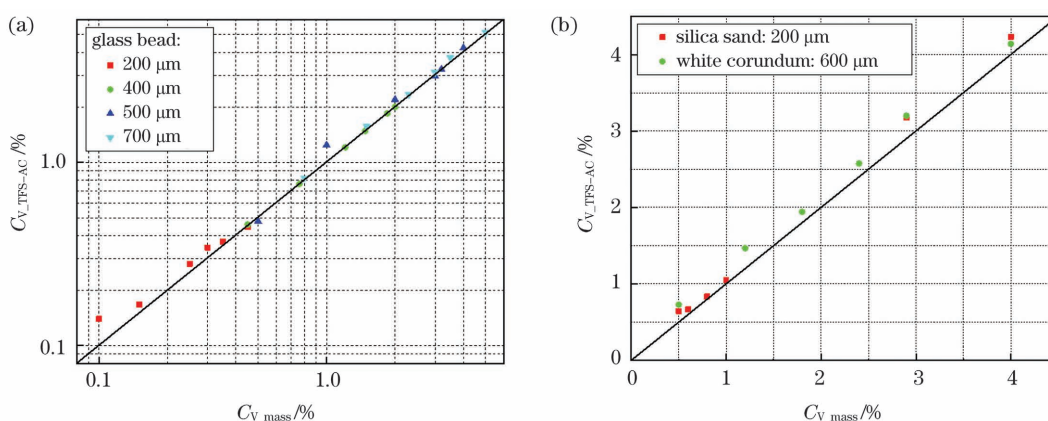


图 6 颗粒体积分数的测量结果。(a)球形玻璃珠;(b)非球形颗粒石英砂和白刚玉

Fig. 6 Measurement results of particle volume fraction. (a) Spherical glass bead; (b) non-spherical silica sand and white corundum

自相关频谱法测量得到的体积分数与称重法得到的体积分数基本吻合。当颗粒为非球形时,体积分数测量结果 $C_{V,TFS-AC}$ 比 $C_{V,mass}$ 稍大,这主要是因为透过率起伏自相关频谱法的理论模型是基于球形颗粒建立的。

在上述实验(见图 2)中,颗粒样品分散在水中,并通过封闭的循环系统由自动循环分散器驱动经过测量

区。在进一步的实验中,采用振动式喂料机替换循环系统,颗粒从给料机出口随机落下并在重力作用下经过测量区,如图 7 所示。由于两光束的中心间隔 $L = 1.4 \text{ mm}$,颗粒经过光束 1 和光束 2 时的速度近似相等。测试对象是标称直径分别为 400、500、900 μm 的玻璃珠以及标称直径为 600 μm 的白刚玉颗粒。

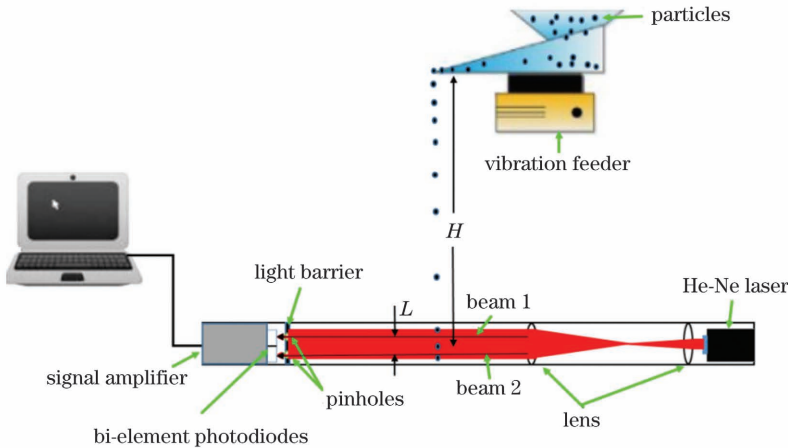


图 7 喂料机给料以及测量示意图

Fig. 7 Schematic of feeding with vibration feeder and measurement

表 4 喂料机给料情况下的颗粒速度测试结果

Table 4 Measurement results on particle velocity under the condition of feeding with vibration feeder

No.	Velocity / ($\text{m} \cdot \text{s}^{-1}$)			
	Glass bead with 400 μm nominal diameter	Glass bead with 500 μm nominal diameter	Glass bead with 900 μm nominal diameter	White corundum with 600 μm nominal diameter
1	1.823 *	1.786 *	2.431	2.692
2	1.923 *	1.823 *	2.778	2.652
3	1.923 *	1.987 *	2.473	2.734
4	2.465	2.459	2.734	2.692
5	2.465	2.433	2.465	2.652

表 4 给出了喂料机给料下 5 次测量得到的速度值,其中:带 * 的速度测量结果对应较小的 H 值(H 值表示喂料机到两光束中心的距离),颗粒的速度较小;不带 * 的速度测量结果对应较大的 H 值,颗粒的速度较大。颗粒经过测量区的速度取决于 H 值($H = 200 \sim 300 \text{ mm}$)。从表 4 所示的测试结果可以看出,速度测试结果具有一定的重复性。由于喂料机振动给料,颗粒在离开喂料机出口时存在随机初速度,因此多

次测量存在较大偏差。

图 8 给出了喂料机给料情况下颗粒粒径累积分布和体积分数的测试结果,相应的特征粒径 x_{10} 、 x_{50} 和 x_{90} 的平均值见表 5。从图 8 可以看出,尽管颗粒流经测量区时的速度存在明显差异,但颗粒粒径分布仍具有较好的重复性。表 5 给出的特征粒径与表 2 相比偏宽,表明颗粒经过测量区时存在一定的速度分布,该速度分布与喂料机出口处颗粒的随机初速度有关。

表 5 喂料机给料情况下特征粒径 x_{10} 、 x_{50} 和 x_{90} 的平均值

Table 5 Average characteristic particle size x_{10} , x_{50} and x_{90} under the condition of feeding with vibration feeder

Particle	$x_{10} / \mu\text{m}$	$x_{50} / \mu\text{m}$	$x_{90} / \mu\text{m}$
Glass bead with nominal diameter of 400 μm	134	385	816
Glass bead with nominal diameter of 500 μm	237	489	847
Glass bead with nominal diameter of 900 μm	402	900	1748
White corundum with nominal diameter of 600 μm	228	579	1288

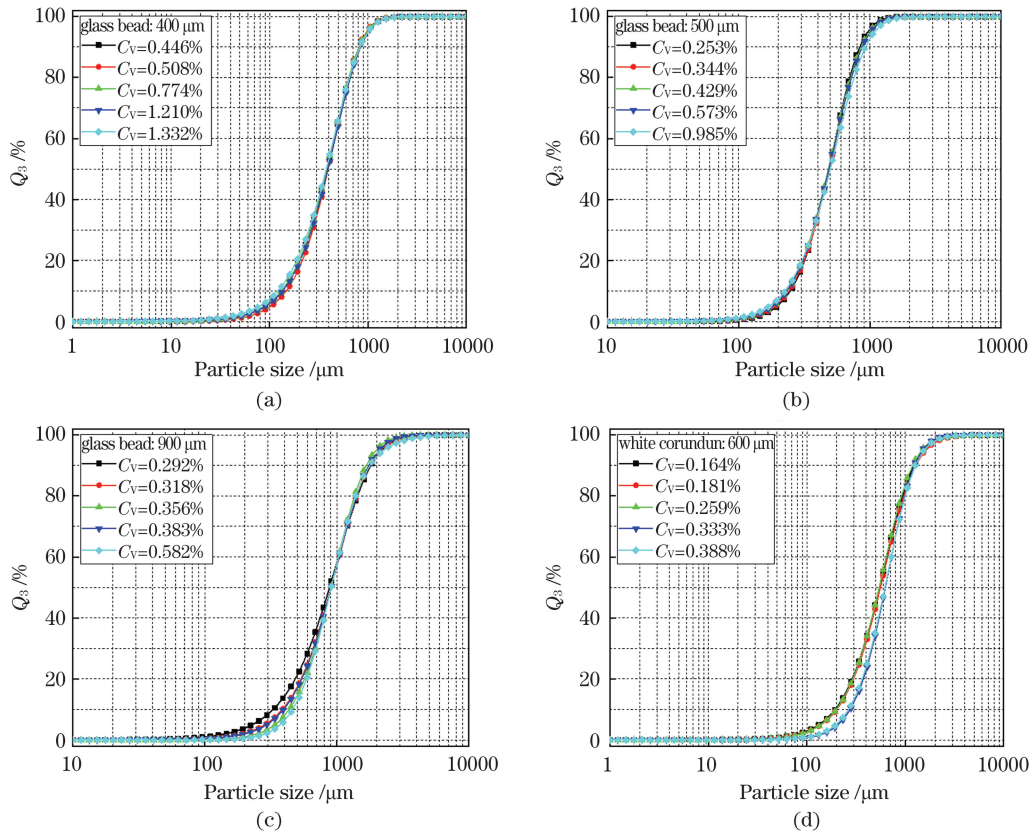


图 8 喂料机给料情况下反演计算得到的粒径累积分布。(a) 标称直径为 $400\text{ }\mu\text{m}$ 的玻璃珠; (b) 标称直径为 $500\text{ }\mu\text{m}$ 的玻璃珠; (c) 标称直径为 $900\text{ }\mu\text{m}$ 的玻璃珠; (d) 标称直径为 $600\text{ }\mu\text{m}$ 的白刚玉

Fig. 8 Inversely calculated particle size cumulative distributions under the condition of feeding with vibration feeder. (a) Glass bead with $400\text{ }\mu\text{m}$ nominal diameter; (b) glass bead with $500\text{ }\mu\text{m}$ nominal diameter; (c) glass bead with $900\text{ }\mu\text{m}$ nominal diameter; (d) white corundum with $600\text{ }\mu\text{m}$ nominal diameter

4 讨论与结论

本文介绍了一种简单的用于实现颗粒粒径分布、体积分数和运动速度同时测量的透过率起伏相关频谱测试装置。采用两束平行光的透过率互相关谱得到颗粒的运动速度，并通过单束光的透过率自相关谱得到颗粒的粒径分布和体积分数。在实际测试中，通过循环分散装置和振动式喂料机两种方式，分别测量了分散在水中(液固两相流)和空气中(气固两相流)的玻璃珠、石英砂和白刚玉颗粒的透过率信号，并获得其透过率相关频谱。最终通过反演计算得到了颗粒的粒径分布、体积分数和运动速度。

受实验条件限制，本次实验中测试的颗粒样品的标称直径在 $200\text{ }\mu\text{m}$ 到 $900\text{ }\mu\text{m}$ 之间，体积分数范围为 $0.1\%\sim 5.2\%$ ，运动速度在 1 m/s 到 3 m/s 之间。从测试原理上讲，透过率起伏相关频谱法可以测试的颗粒粒径的上限不受限制。粒径越大，颗粒引起的透过率起伏信号越强，频谱信号质量越好；但粒径测量的下限受光束直径的限制，当颗粒粒径远小于光束直径时，透过率起伏信号变得非常微弱，自相关频谱信号质量变差。通常取光束直径的 $1/10$ 作为颗粒粒径的测量下限。本次实验中的光束直径为 $850\text{ }\mu\text{m}$ ，可测量的粒

径下限约为 $85\text{ }\mu\text{m}$ 。如要测量更小的颗粒，可采用会聚的高斯光束^[16,18]，以减小光束宽度。另外，本文采用的理论模型是基于单散射构建的，适用于透过率期望值不低于 0.5 的情况，这决定了颗粒体积分数的测量上限。对于高体积分数颗粒样品的测量，需要在理论模型中增加颗粒体积分数修正模块。颗粒体积分数的测量下限与透过率期望值 0.95 对应，若颗粒体积分数过低，透过率起伏相关谱的质量会变差，不易得到可靠的测量结果。根据式(4)和式(6)，在相同的透过率下，不同粒径的颗粒对应不同的颗粒体积分数。因此，颗粒体积分数测量上限和下限与颗粒粒径有关。在本次实验中，透过率大致处于相同的范围，因此对不同粒径样品的测量体积分数分别在不同的范围内。颗粒流速的测量范围主要取决于采样频率和两路信号的空间间隔，实验中两路信号的空间间隔为 1.4 mm ，颗粒速度范围在 1 m/s 至 3 m/s 之间，故采样频率设置为 125 kHz 。如果要测量更高的流速，可适当提高采样频率，必要时减小两路信号的间距。

在理论模型中，假定颗粒是球形的，而且测量过程中每组样品的所有颗粒均以恒定的速度流动。非球形颗粒的测量结果与颗粒流经测量区的取向(姿态)有关。两相流中颗粒体积分数的反演结果与颗粒的球形

度有关,应考虑对球形度进行修正。当颗粒在流场中出现速度分布或者流场不稳定时,测量得到的速度值是测量时段内所有颗粒速度的平均值。受流速测量结果的影响,颗粒粒径分布宽度测试结果比实际结果更宽。为了避免流速分布和变化对测量结果产生影响,一方面可以考虑控制流场的稳定性,另一方面可以提高采样频率并缩短单次测量的时间。

本次研究表明,透过率起伏相关频谱法的测试结果与样品的标称直径、其他测试方法所得结果吻合。实验研究初步验证了该测试方法和测试装置的可行性和测试结果的重复性。本文介绍的测试装置具有结构简单、易实现和易维护的特点,有望应用于颗粒两相流的在线测量。

参 考 文 献

- [1] Stanley-Wood N G, Llewellyn G J, Taylor A. On-stream particle size, concentration and velocity measurements by auto-correlation of scattered laser light [J]. Powder Technology, 1981, 29(2): 217-223.
- [2] 崔方晓, 李大成, 吴军, 等. 基于Lasso方法的污染气体自适应探测算法[J]. 光学学报, 2019, 39(5): 0530003
- Cui F X, Li D C, Wu J, et al. Adaptive feature extraction algorithm based on Lasso method for detecting polluted gas[J]. Acta Optica Sinica, 2019, 39(5): 0530003
- [3] Yong Y. Mass flow measurement of bulk solids in pneumatic pipelines[J]. Measurement Science and Technology, 1996, 7(12): 1687-1706.
- [4] Zhang S F, Zhang Q H, Shang J Z, et al. Measurement methods of particle size distribution in emulsion polymerization [J]. Chinese Journal of Chemical Engineering, 2021, 39: 1-15.
- [5] 尹朝阳, 张德志, 赵林杰, 等. 大口径反射镜表面颗粒污染物暗场检测算法研究[J]. 光学学报, 2020, 40(7): 0711003
- Yin Z Y, Zhang D Z, Zhao L J, et al. A dark-field detection algorithm to detect surface contamination in large-aperture reflectors[J]. Acta Optica Sinica, 2020, 40(7): 0711003.
- [6] Zheng E Z, Rudman M, Kuang S B, et al. Turbulent coarse-particle non-Newtonian suspension flow in a pipe [J]. International Journal of Multiphase Flow, 2021, 142: 103698.
- [7] 王建国. 机制砂粒径分布对混凝土拌合物性能的影响研究[J]. 建筑技术开发, 2020, 47(23): 140-141.
- Wang J G. Influence of particle size distribution of manufactured sand on performance of concrete mixture [J]. Building Technology Development, 2020, 47(23): 140-141.
- [8] 梁明, 杨维仁, 吕爱军. 粉碎粒度对制粒和畜禽生产性能的影响[J]. 饲料博览, 2011(9): 30-32.
- Liang M, Yang W R, Lü A J. Effects of particle size on pelletizing and growth performance of livestock and poultry [J]. Feed Review, 2011(9): 30-32.
- [9] Laceby J P, Evrard O, Smith H G, et al. The challenges and opportunities of addressing particle size effects in sediment source fingerprinting: a review [J]. Earth-Science Reviews, 2017, 169: 85-103.
- [10] Yu H, Tan C, Dong F. Measurement of particle concentration by multifrequency ultrasound attenuation in liquid-solid dispersion [J]. IEEE Transactions on Ultrasonics, Ferroelectrics, and Frequency Control, 2021, 68(3): 843-853.
- [11] Chen X Z, Zhou W, Cai X S, et al. In-line imaging measurements of particle size, velocity and concentration in a particulate two-phase flow[J]. Particuology, 2014, 13(2): 106-113.
- [12] Xiao H R, Yao Y G, Liu X D, et al. Solid particle flow characteristics in the cone valve and its flow rate prediction model[J]. Chemical Engineering Research and Design, 2021, 175: 330-338.
- [13] den Moortel T V, Azario E, Santini R, et al. Experimental analysis of the gas-particle flow in a circulating fluidized bed using a phase Doppler particle analyzer [J]. Chemical Engineering Science, 1998, 53(10): 1883-1899.
- [14] Prasad S, Schweizer C, Bagaria P, et al. Investigation of particle density on dust cloud dynamics in a minimum ignition energy apparatus using digital in-line holography [J]. Powder Technology, 2021, 384: 297-303.
- [15] 苏明旭, 周健明, 汪雪, 等. 超声谱法在颗粒两相流测量中的应用进展[J]. 中国粉体技术, 2016, 22(5): 22-27.
- Su M X, Zhou J M, Wang X, et al. Developments and applications of ultrasound spectroscopy in particle characterization[J]. China Powder Science and Technology, 2016, 22(5): 22-27.
- [16] Shen J Q, Riebel U, Guo X A. Measurements of particle-size distribution and concentration by transmission fluctuation spectrometry with temporal correlation [J]. Optics Letters, 2005, 30(16): 2098-2100.
- [17] 沈建琪, 蔡小舒, 于彬. 消光起伏自相关频谱法颗粒测量技术[J]. 工程热物理学报, 2006, 27(5): 795-798.
- Shen J Q, Cai X S, Yu B. Particle sizing by transmission fluctuation auto-correlation spectrometry [J]. Journal of Engineering Thermophysics, 2006, 27(5): 795-798.
- [18] Shen J Q, Yu B, Xu Y M, et al. Particle analysis by transmission fluctuation spectrometry with temporal correlation in multiphase flow[J]. Flow Measurement and Instrumentation, 2007, 18(3/4): 166-174.
- [19] Guo X A, Riebel U, Shen J Q. Particle size analysis by transmission fluctuation spectrometry: theory and simulations on the spatial correlation technique [C]//Proceedings of 2004 PARTEC International Congress for Particle Technology, March 16-18, 2004, Nürnberg, Germany. [S.l.: s.n.], 2004.
- [20] Shen J Q, Riebel U, Guo X A. Transmission fluctuation spectrometry with spatial correlation [J]. Particle & Particle Systems Characterization, 2005, 22(1): 24-37.
- [21] Ferri F, Bassini A, Paganini E. Modified version of the Chahine algorithm to invert spectral extinction data for particle sizing[J]. Applied Optics, 1995, 34(25): 5829-5839.
- [22] 王晨, 张彪, 曹丽霞, 等. 颗粒粒径分布测量反演算法的改进[J]. 光学学报, 2019, 39(2): 0212009.
- Wang C, Zhang B, Cao L X, et al. An improved inversion algorithm to measure particle size distribution[J]. Acta Optica Sinica, 2019, 39(2): 0212009.
- [23] 王天恩, 沈建琪, 林承军. 前向散射颗粒粒径分布分析中的向量相似度反演算法[J]. 光学学报, 2016, 36(6): 0629002.
- Wang T E, Shen J Q, Lin C J. Vector similarity retrieval algorithm in particle size distribution analysis of forward scattering[J]. Acta Optica Sinica, 2016, 36(6): 0629002.
- [24] 王雅静, 窦智, 申晋, 等. TSVD-Tikhonov正则化多尺度动态光散射反演[J]. 中国激光, 2017, 44(1): 0104003.
- Wang Y J, Dou Z, Shen J, et al. Multi-scale inversion combining TSVD-Tikhonov regularization for dynamic light scattering[J]. Chinese Journal of Lasers, 2017, 44 (1): 0104003.
- [25] 张杰, 蔡小舒, 周骜. 图像动态光散射法纳米颗粒粒度分布反演算法研究[J]. 光学学报, 2016, 36(9): 0929001.
- Zhang J, Cai X S, Zhou W. Nanoparticle size distribution inversion algorithm in image dynamic light scattering[J]. Acta Optica Sinica, 2016, 36(9): 0929001.

Measurement of Particle Velocity, Particle Size Distribution, and Particle Volume Fraction in Two-Phase Flow Using Transmission Fluctuation Correlation Spectrometry

Gong Peng, Shen Jianqi*

College of Science, University of Shanghai for Science and Technology, Shanghai 200093, China

Abstract

Objective Particle-fluid two-phase flows exist widely in energy, industry, environment, and other fields. Thus, it is important to simultaneously determine the parameters of two-phase flow, such as the particle size distribution, volume fraction, and flow velocity. For example, in a thermal power plant, the particle size distribution of pulverized coal and its feed flow are critical issues in ensuring combustion efficiency and reducing pollutant emissions. In mineral processing and feed manufacturing, real-time measurement of these parameters is important for maintaining stable conditions to ensure the quality of products. It is also important in other applications, such as pipeline transportation using air as the carrier medium, in which real-time monitoring of flow velocity is necessary. With the development of science and technology, different online measurement techniques have been proposed and used to measure the parameters of particles in a two-phase flow, including ultrasonic spectrometry, image methods, and digital holography. However, some techniques are limited in their applications because their measurements can be affected by poor environmental conditions. In principle, ultrasonic spectrometry requires several particle and dispersion parameters, which are usually unavailable. Digital holographic technology employs a complicated optical setup that can be easily contaminated by dust. In addition, this technique is suitable only for measuring low particle volume fractions. Therefore, there is an urgent need to develop a simple measurement setup for real-time and online (or inline) measurements of the particle parameters of two-phase flows.

Methods Transmission fluctuation correlation spectrometry (TFCS) is an optical measurement technique that utilizes the autocorrelation characteristics of transmission fluctuation signals of a narrow light beam to obtain information on particle size distribution and volume fraction. In this study, a simple beam-splitting setup was used, which produced two parallel narrow beams, allowing the detection of two channels of transmission signals for further correlation of the transmission fluctuations. Compared with a method that uses only one light beam, this optical setup can measure two channels of transmission fluctuation signals; therefore, cross-correlation spectra of these signals may be obtained, from which particle velocities can be extracted. In addition, the auto-correlation spectra of the transmission fluctuations of either or both channels can be calculated to obtain information on the particle size distribution and volume fraction.

Results and Discussions Experiments are performed using spherical/non-spherical particles dispersed in water. The nominal diameters of the samples range from 200 to 900 μm . In the first part of the measurements (Fig. 2), the suspension of the particles is driven by a pump (BT-800) and circulates in a closed system at a constant flow velocity of approximately 1.15 m/s in the measuring zone, which is measured using a laser velocimeter (TM680). The He-Ne laser beam is expanded and collimated at a diameter of approximately 8 mm. The light beam propagates along the direction normal to the particle flow, and a bi-element photodiode (S4204) is employed to measure the transmitted signals. Two pinholes are installed in front of the photodiode. The diameter of the pinholes is 850 μm and the distance between their centers is 1.4 mm. The signals are amplified and recorded using a multichannel A/D card (PCI-50612). The sampling time for each measurement is 4.096 s, and the sampling frequency is 125 kHz. The second part of the measurements uses the same optical setup; however, the particles are fed by a vibrator (Fig. 7). Under gravity, the particles pass through the measurement zone at a constant velocity. The cross-correlation spectra of the transmission signals of the channels and the autocorrelation spectra of the transmission signals of a single channel are calculated using the fast Fourier transform (FFT). The delay time of the cross-correlation spectrum corresponding to the peak of the spectrum is used to extract the velocity of the particles. The results (Table 1) agree with those obtained using a laser velocimeter. The relative errors range from -8.8% to 0.95%. The particle size distribution and volume fraction are extracted from the autocorrelation spectrum. A modified Chahine iteration algorithm is used for the inverse calculation. The mean particle sizes x_{50} (Table 2) of the measured samples agree with the nominal diameters. All samples are also measured using a laser particle analyzer (Bettersize2600). It is found that the mean particle sizes x_{50} measured using the proposed TFCS (Table 2) agree well with those of the laser particle analyzer (Table 3); the relative error range from 0.1% to 5%. However, the sizes of x_{10} and x_{90} obtained using the TFCS (Fig. 5 and Table 2) differ significantly from those of the laser particle analyzer

(Table 3). This difference is caused mainly by the distribution of the velocity of the particles when they pass through the measurement zone owing to the flow condition and the pulse caused by the pump. The measured particle volume fractions are compared with those based on the known weights of the samples (Fig. 6). A good agreement is achieved between the two sets of values for spherical particles [Fig. 6 (a)]. However, for non-spherical particles, the volume fractions obtained using the TFCS are higher than those based on the weights of the samples [Fig. 6(b)], which means that shape correction is required. All measurements are repeated several times, and the results for particle velocity, particle size distribution, and volume fraction show good repeatability. Data processing, including computation of the spectra and inversion, can be completed within 3–5 s. Thus, the proposed measurement is useful for real-time applications.

Conclusions This study introduces a simple optical setup for transmission fluctuation correlation spectrometry, which can be used to simultaneously measure particle velocity, particle size distribution, and volume fraction. Two parallel narrow light beams are produced to measure transmission fluctuations and obtain autocorrelation of the signals of a single beam and cross-correlation of the signals of two beams. The particle velocity is obtained from the transmission cross-correlation spectrum, and the particle size distribution and volume fraction are deconvoluted from the autocorrelation spectrum.

The measurements are implemented using both spherical and nonspherical particles, and the TFCS results are compared with those obtained using other methods. The results show good agreement and repeatability. The measurement and subsequent data processing can be completed within 10 s. Therefore, the proposed setup is promising for use in real-time and online applications in particle-fluid two-phase flows.

Key words measurement; two-phase flow; transmission fluctuation correlation spectrometry; particle-size distribution